Neutron diffraction study of the chiral magnet MnGe

O. L. Makarova,[1,2] A. V. Tsvyashchenko,[3] G. Andre,[1] F. Porcher,[1] L. N. Fomicheva,[3] N. Rey,[1] and I. Mirebeau[1,*]

[1]*CEA, Centre de Saclay, DSMI, RAMIS, Laboratoire Léon Brillouin, 91191 Gif-sur-Yvette, France*

[2]*National Research Center "Kurchatov Institute," 123182 Moscow, Russia*

[3]*Vereshchagin Institute for High Pressure Physics, Russian Academy of Sciences, 142190 Troitsk, Russia*

(Received 9 August 2011; revised manuscript received 14 March 2012; published 14 May 2012)

The magnetic structure of cubic MnGe has been determined by powder neutron diffraction. MnGe has a helical spin structure with a propagation vector $\mathbf{k} = (0,0,\zeta)$, where $\zeta = 0.107(5)$ just below the transition temperature $T_N = 170$ K. The ζ value increases upon cooling and locks in to the value of 0.167(4) below 30 K. The moment value is $2.3(5)\mu_B$ at 2 K. The onset of the magnetic order is connected with a symmetry lowering from cubic to orthorhombic.

DOI: 10.1103/PhysRevB.85.205205 PACS number(s): 75.30.Kz, 75.76.+j, 75.25.−j, 75.30.−m

Uncollinear magnets yield the possibility of coupling electric and magnetic degrees of freedom, a key ingredient for building novel electronic devices. This process is at play in the so-called type-II multiferroic materials where the coupling between electric and magnetic order parameters, arising from inverse Dzyaloshinskii-Moriya[1] (DM) or exchange striction mechanisms, allows one to control the electric polarization by a magnetic field and vice versa.

Other examples of uncollinear magnets where the DM energy is at play are the itinerant magnets with $B20$ cubic crystal structure and helical magnetic structure such as MnSi. MnSi, where a helical ordering is stabilized below $T_N = 29.5$ K, has attracted a lot of interest due to its unusual magnetic and transport properties.[2] A quantum critical transition toward a non-Fermi-liquid state occurs under pressure,[3] as well as a peculiar spin texture under a magnetic field. Under a moderate applied field in the range 0.1–0.6 T, the helical spin structure of MnSi becomes noncoplanar, and topological field configurations, the so-called Skyrmion lattice where the spin direction wraps a sphere, are stabilized near the transition.[4–6] This phenomenon is the source of a topological Hall effect (THE), similar to that initially observed in spin glasses[7] and frustrated pyrochlores.[8] In this process, conduction electrons hopping over three sites of noncoplanar localized magnetic moments acquire a Berry phase as they follow adiabatically the polarization of these topologically stable knots. The Berry phase is directly related to the scalar spin chirality $\mathbf{S}_i \cdot (\mathbf{S}_j \times \mathbf{S}_k)$ and to the amplitude of the Hall effect.[9,10]

In the cubic $B20$ compounds of space group (SG) $P2_13$, the helical spin order is due to the competition between the ferromagnetic exchange interaction and DM anisotropy, which can occur because of the lack of centrosymmetry of the structure.[11] Anisotropic exchange, dipolar interactions, and cubic crystal field anisotropy also play roles in determining the characteristics of the helical structure.[12–15] In an applied field, the density of Skyrmions and the magnitude of the THE are theoretically proportional to the squared period of the helical modulation.[9] Decreasing this period by chemical substitution may promise a higher density of Skyrmions if realized in a magnetic field.

With respect to MnSi, MnGe offers the possibility of decreasing the helical period. Up to now, very few studies have been performed in MnGe since its synthesis is quite complex and only powdered samples are available. An early work[16] showed a metallic behavior with a change of slope in the resistivity and a maximum of the thermoelectric power around 170 K, whereas the susceptibility peaked 27 K higher. In very recent work[17,18] a broad antiferromagnetic peak of the susceptibility was observed around $T_N = 170(5)$ K, in agreement with results from powder neutron diffraction. MnGe shows a Curie-Weiss behavior below 300 K with an effective Mn magnetic moment of $3.68\mu_B$ close to the effective moment of $3.87\mu_B$ expected for the Mn^{4+} ion and a Curie-Weiss constant $\theta_{CW} = +231$ K (where the $+$ sign corresponds to ferromagnetic interactions). It also shows the largest THE response among the $B20$ chiral magnets.

We investigated the crystal structure of MnGe by high-resolution powder neutron diffraction. We also studied the magnetic structure versus temperature with great accuracy, using cold neutrons to observe the satellite of the $Q = 0$ reflection, expected for this type of helical order but unobserved before to our knowledge. We show that the crystal and magnetic structures are closely connected, so that the spiral structure is concomitant with a lattice distortion. The MnGe helical order is compared with that of MnSi.

A polycrystalline sample of MnGe was synthesized at 8 GPa in a toroidal high-pressure apparatus by a melting reaction with Mn and Ge. The Mn purity was 99.0% and that of Ge 99.999%. The pellets of well-mixed powdered constituents were placed in rocksalt pipe ampoules and then directly electrically heated to 1600 °C. Then the samples were quenched to room temperature before the applied pressure was released.[19]

Room-temperature x-ray diffraction shows that MnGe crystallizes in the cubic $B20$-type structure, with a cell parameter $a = 4.806(5)$ Å. Impurity phases of $Mn_{11}Ge_8$ and Mn_2O_3 with a total amount of less than 5% of the main phase were identified. Powder neutron diffraction experiments were carried out at the Laboratoire Léon Brillouin on the powder diffractometer G4-1 (with incident neutron wavelength $\lambda = 2.42$ Å) and the diffractometer G6-1 ($\lambda = 4.74$ Å). The magnetic and crystal structures were analyzed with the FULLPROF program based on the Rietveld method.[20]

Figure 1 shows the refined diffraction patterns recorded at 220 and 2 K on the G4-1 diffractometer. In the paramagnetic

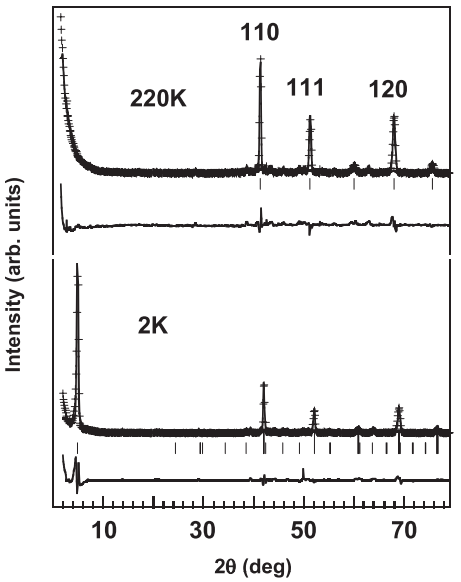

FIG. 1. Observed (+), calculated (solid line), and difference (solid line below) neutron diffraction patterns of MnGe measured on the G4-1 diffractometer ($\lambda = 2.42$ Å). Tick marks show the positions of the Bragg reflections in cubic notation.

range [above $T_N = 170(5)$ K], the diffraction patterns are well refined by assuming the cubic $B20$ structure of space group $P2_13$. Both Mn and Ge atoms are situated at the positions (x,x,x) of the $4a$ sites, and the refined values $x_{\mathrm{Mn}} = 0.136$ and $x_{\mathrm{Ge}} = 0.846$ are close to those previously obtained.[16] At low temperature, the helical magnetic order is clearly evidenced by an intense satellite of the $Q = 0$ reflection, the so-called zero satellite, clearly seen in the low-angle region of the diffraction patterns. Satellites of the nuclear Bragg peaks with much weaker intensity are also observed, as shown on the magnetic patterns measured on G6-1 (Fig. 2 right). No magnetic contribution is found in the nuclear Bragg peaks. Figure 2 shows the temperature evolution of the strong zero satellite (left) and of the weak satellites of the 110 reflection (right). All magnetic reflections can be indexed with an

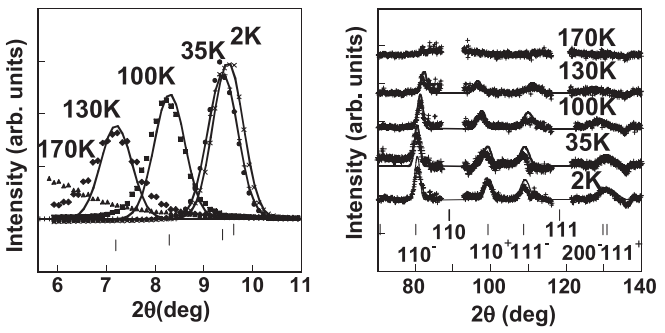

FIG. 2. Neutron diffraction patterns measured on the G6-1 diffractometer ($\lambda = 4.74$ Å). Left: temperature evolution of the zero satellite. Right: temperature evolution of the satellites of the 110 and 111 Bragg reflections. Solid lines are refinements as described in the text. The magnetic patterns on the right are obtained by subtracting a pattern in the paramagnetic region. Tick marks show the positions of the Bragg reflections in cubic notation.

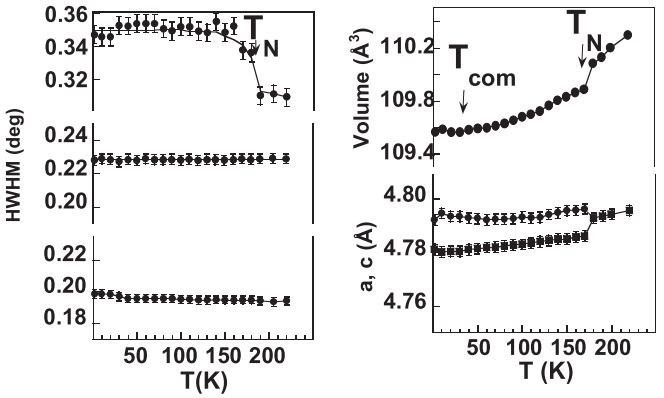

FIG. 3. Left: temperature dependencies of the half width at half maximum (HWHM) of three nuclear Bragg reflections. Right: temperature dependencies of the lattice parameters $a = b$ and c, and of the unit cell volume.

incommensurate wave vector $\mathbf{k} = (0,0,\zeta)$ in reciprocal lattice units, with $\zeta = 0.107(5)$ just below T_N. The ζ component of the wave vector increases upon cooling and reaches the value 0.167(4) at 30 K. Then it does not change below 30 K.

A careful comparison of the diffraction patterns measured at temperatures below and above the magnetic transition strongly suggests that the magnetic transition is accompanied by a small lattice distortion. This effect is shown by plotting the linewidth of the nuclear Bragg peaks (Fig. 3, left) versus temperature. The diffraction patterns measured on G4-1 allow us to measure three nuclear Bragg peaks indexed as 110, 111, and 120 in the cubic unit cell. The 120 Bragg peaks shows a broadening of the linewidth of about 2% between 280 and 2 K. A very small broadening of the 110 Bragg is also suggested, whereas the linewidth of the 111 Bragg peak remains constant in the whole temperature range. We interpret the broadening of the nuclear Bragg peaks as a splitting due to symmetry lowering, too small to be resolved by the experimental resolution of the diffractometer. Considering that the 111 peak does not split, we assume that this symmetry lowering stabilizes an orthorhombic structure. We then refined our data by considering an orthorhombic unit cell with two identical or nearly identical a,b lattice parameters, different from c. The temperature dependencies of the lattice parameters and volume are shown on Fig. 3, right. The refinement shows that the orthorhombic splitting and volume anomaly occur at the magnetic transition $T_N = 170$ K. The transition at T_N is accompanied by a small volume effect $\frac{\delta V}{V} = 0.02\%$. A second small volume anomaly is suggested at $T_{\mathrm{com}} = 30$ K.

To determine the crystal structure completely, we refined high-resolution powder diffraction patterns measured at three temperatures (200, 50, and 6 K), considering either the cubic or the orthorhombic unit cell. At 200 K (above T_N) the best refinements were obtained by considering a cubic unit cell and anisotropic atomic displacements of Mn and Ge atoms. Below T_N, such refinements yielded strongly anisotropic thermal displacement parameters, with ratios above 20 between them which seemed unphysical. Therefore a model assuming an

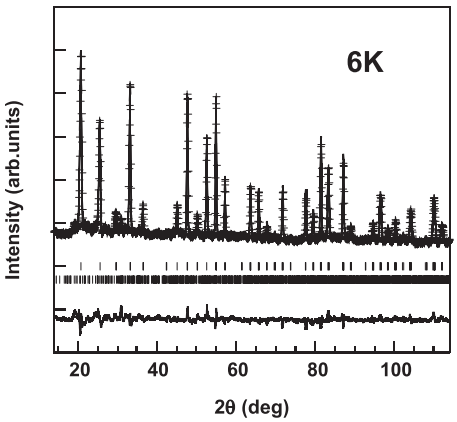

FIG. 4. High-resolution neutron diffraction pattern of MnGe at 6 K, measured on the 3T2 diffractometer. Tick marks show the positions of the Bragg reflections. The refinement is made in the orthorhombic unit cell (SG $P2_12_12_1$).

orthorhombic unit cell was adopted. In the orthorhombic basis, we assumed that the thermal displacements were isotropic.

The refined pattern at 6 K is shown in Fig. 4. The atomic positions, thermal parameters, and lattice constants deduced from the structural refinements at 200, 50 , and 6 K are given in Table I.

The magnetic structure was refined in the orthorhombic unit cell. We notice that the orthorhombic space group $P2_12_12_1$ is a nonisomorphic subgroup of the cubic space group $P2_13$, both groups allowing a propagation vector of the type $(0,0,\zeta)$. The temperature variations of ζ and of the the helical wavelength l related to the modulus of the wave vector[5,14] by $l = 2\pi/\zeta$ are shown in Fig. 5 left. Below $T_{com} = 30$ K, the wave vector saturates to the wave vector $\mathbf{k} = (0,0,0.167(4))$. The

TABLE I. Crystal structure parameters of MnGe, deduced from the refinements of the high-resolution neutron diffraction patterns measured on 3T2.

		200 K	50 K	6 K
Space group		$P2_13$	$P2_12_12_1$	$P2_12_12_1$
Lattice parameters				
a (Å)		4.7925(25)	4.7808(24)	4.7806(30)
b (Å)			4.7807(22)	4.7805(29)
c (Å)			4.7938(30)	4.7939(10)
Atomic coordinates and thermal displacement parameters				
Mn 4a				
	x	0.136(30)	0.145(40)	0.142(12)
	y		0.129(41)	0.131(16)
	z		0.136(36)	0.136(11)
	B (Å^2)	1.2(9)	0.59(12)	0.51(9)
Ge 4a				
	x	0.846(9)	0.846(9)	0.845(6)
	y		0.843(9)	0.843(7)
	z		0.843(8)	0.842(6)
	B (Å^2)	0.9(4)	0.24(3)	0.24(3)
Reliability factors				
R_p (%)		4.3	5.3	6.3
R_{exp} (%)		2.6	2.4	2.4

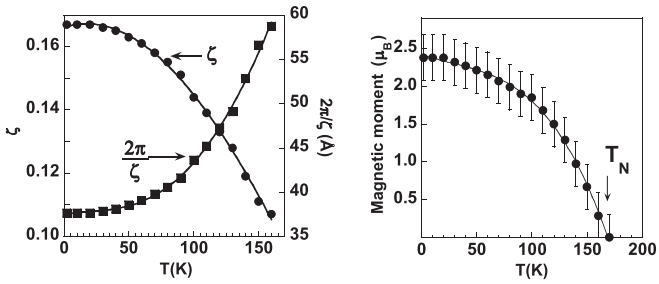

FIG. 5. Left: temperature variations of the ζ component of the wave vector $\mathbf{k} = (0,0,\zeta)$ and helical wavelength $2\pi/\zeta$. Right: temperature dependence of the ordered Mn magnetic moment.

commensurate wave vectors $(0,0,\frac{1}{6})$ and $(0,0,\frac{4}{25})$ are equally compatible with this low-temperature wave vector within the experimental accuracy.[21]

The absence of a magnetic contribution to the nuclear peaks and the presence of first-order satellites favors a helical structure rather than a conical one. We have checked that an amplitude modulation of the structure like a sinusoidal modulation of the Mn magnetic moments yields a worse agreement with the data. The best refinement ($R_{mag} = 9\%$ at 2 K) was obtained by considering a helix propagating along the c axis with Mn moments in the (a,b) plane. A comparison of the calculated and observed integrated intensities measured at at 2 K on G4-1 diffractometer is given in Table II. The temperature dependence of the Mn magnetic moment is shown in Fig. 5, right. The Mn moment reaches $2.3(5)\mu_B$ at 2 K, to be compared with the value of $3\mu_B$ expected for ionic Mn^{4+}.

To summarize, the most intriguing features of the MnGe magnetic structure, which contrast with those of MnSi, are (i) a much higher magnetic transition $T_N = 170$ K and ordered Mn moment $M_0 = 2.3\mu_B$ at $T = 0$, instead of $T_N = 29.5$ K and $M_0 = 0.4\mu_B$ in MnSi; (ii) a much smaller helical wavelength:

TABLE II. Comparison of the calculated and observed integrated intensities of the hkl reflections measured at 2 K on G4-1. Top, nuclear reflections; bottom, magnetic satellites. The interplanar spacings d_{hkl} are also given.

hkl	d_{hkl} (Å)	I_{calc}	I_{obs}
101	3.385(1)	1759	1900
110	3.380(1)	926	1038
111	2.763(1)	1551	1816
012	2.143(1)	683	832
201	2.139(1)	698	685
210	2.138(1)	680	704
000(−)	28.706(1)	9400	12600
101(+)	3.677(1)	136	153
101(−)	3.116(1)	84	176
111(+)	2.915(1)	92	140
111(−)	2.610(1)	60	120
012(+)	2.294(1)	72	208
201(+)	2.208(1)	74	34
012(−)	2.066(1)	56	10
201(−)	2.004(1)	32	16

40 Å instead of 180 Å in MnSi; (iii) a strong temperature dependence of the helical wavelength; (iv) a lattice distortion which occurs together with the helical structure; (v) a lock-in transition at a lower temperature $T_{com} = 30$ K where the ζ component of the wave vector locks in to the value 0.167(4).

In MnSi and FeGe,[22,23] the spontaneous ordered moments are much smaller ($0.4\mu_B$ and $1\mu_B$, respectively) than the effective moments deduced from the Curie-Weiss susceptibility (respectively $1.4\mu_B$ and $3\mu_B$). Paramagnetic fluctuations and Curie-Weiss behavior can be explained in the frame of itinerant-electron magnetism by self-consistent renormalization theory,[24] and a strong moment reduction can be derived from band structure calculations.[25] Substituting Mn or Fe for Co yields compounds with similar helical structures.[26,27] Interestingly, FeGe and $Fe_xCo_{1-x}Si$ with higher T_N values than MnSi (50 K in $Fe_{0.5}Co_{0.5}Si$ and 270 K in FeGe) also have longer helical wavelengths ($l = 500$ to 1000 Å). In $Fe_xMn_{1-x}Si$ alloys as well, smaller T_N values coincide with smaller helical wavelengths than in MnSi.

MnGe shows a very different behavior, since the high T_N and magnetic moment values are associated with the smallest helical wavelength (40–60 Å) of the *B*20 family. Within a Landau description of the free energy,[11–14] the stabilization of the helix is explained by a competition between ferromagnetic isotropic exchange and antisymmetric DM interactions, the latter arising from the noncentrosymmetric atomic arrangement. The helical wavelength l is determined by the ratio of the exchange energy A and strength of the DM interaction D ($l = 4\pi A/D$).[15]

According to this expression, and assuming that A roughly scales with T_N in the *B*20 family, the high T_N value of MnGe combined with its small helical wavelength suggests a much higher DM energy and spin-orbit coupling constant g_{SO} than in the other *B*20 compounds. The DM interaction which leads to incommensurate order is of second order in g_{SO}. This constant having almost no temperature dependence, the DM term alone cannot lead to a temperature-dependent helical period and lock-in transition. So weaker energy terms should be at play, which are invariant under the symmetry operators of the crystal space group. As shown in Ref. 14, in the *B*20 alloys, the crystal field terms at fourth order in g_{SO} can pin the helix along privileged crystal axes and induce a lock-in transition.

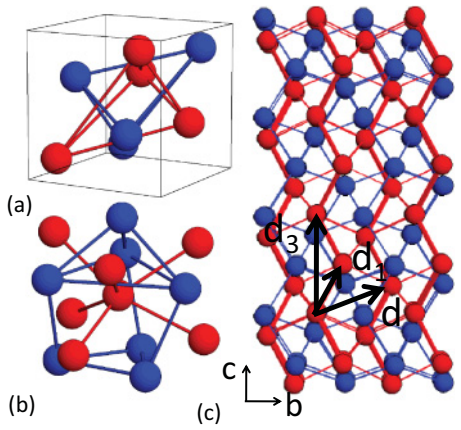

FIG. 6. (Color online) (a) Crystal structure of MnGe. Red and blue balls correspond to Mn and Ge atoms. (b) Coordination polyhedron of Mn. (c) Projection of the crystal structure along [001]; arrows indicate the typical Mn-Mn distances in the unit cell.

TABLE III. Near-neighbor interatomic distances d (Å) for Mn-Mn, Ge-Ge, and Mn-Ge pairs, calculated from the refined atomic positions of Table I.

	200 K	50 K	6 K
d_{Mn-Mn}	2.938(5)	2.88(3)	2.89(2)
		2.96(3)	2.95(3)
		2.97(3)	2.96(3)
d_{Ge-Ge}	2.967(2)	2.944(11)	2.947(12)
		2.964(11)	2.967(12)
		2.973(13)	2.969(11)
d_{Mn-Ge}	2.431(4)	2.43(2)	2.430(20)
	2.500(4)	2.45(2)	2.470(20)
	2.692(4)	2.51(2)	2.508(17)
		2.53(2)	2.530(20)
		2.55(3)	2.650(30)
		2.63(3)	2.700(20)
		2.70(3)	2.701(17)

The onset of a structural transition at T_N may also be related to the spin-orbit interaction, as in some multiferroics.[1]

Finally, considering the *B*20 crystal structure as shown in Fig. 6, and the near-neighbor distances deduced from the refinement, as reported in Table III, one notices that three typical Mn-Mn distances (of about 2.95, 4.37, and 4.78 Å) exist in the cubic unit cell. In a localized approach, it could induce different magnitudes for the exchange interactions between near-neighbor Mn moments and perhaps tune the helical wavelength.[28] A localized approach has already been considered for several compounds of the Mn-Ge system with different crystal and magnetic structures.[29]

All these features call for an original interaction scheme in MnGe, possibly at the borderline of localized and itinerant magnetism. Theoretical models are now needed to account for this behavior in a quantitative way.

In conclusion, we have performed a powder neutron diffraction study of the magnetic structure of MnGe. Below 170(5) K MnGe has a helical spin structure, with high ordered moment. The high transition temperature together with the short helical wavelength suggest a strong enhancement of the DM interaction with respect to the other compounds of the *B*20 family. The helical wavelength changes with temperature and the structure possibly locks in to a commensurate structure below 30 K. The onset of the helical order coincides with a symmetry lowering. All these features reflect an original behavior, still to be understood theoretically.

This work was supported by the Russian Foundation for Basic Research (Grant No. 11-02-00029), the Program of the Presidium of RAS "Physics of Strongly Compressed Matter," and by Le Triangle de la Physique. We are grateful to S. M. Stishov for supporting this work, to him, S. Grigoriev, E. Moskvin, Y. Sidis, D. Lamago, A. Gukasov, and A. V. Irodova for interesting discussions, and to P. Bonville for a critical reading of the manuscript.

*isabelle.mirebeau@cea.fr

[1] H. Katsura, N. Nagaosa, and A. V. Balatsky, Phys. Rev. Lett. **95**, 057205 (2005).

[2] A. Hamann, D. Lamago, Th. Wolf, H. V. Löhneysen, and D. Reznik, Phys. Rev. Lett. **107**, 037207 (2011).

[3] C. Pfleiderer, S. R. Julian, and G. G. Lonzarich, Nat. (London) **414**, 427 (2001).

[4] A. Neubauer, C. Pfleiderer, B. Binz, A. Rosch, R. Ritz, P. G. Niklowitz, and P. Böni, Phys. Rev. Lett. **102**, 186602 (2009).

[5] C. Pappas, E. Lelièvre-Berna, P. Falus, P. M. Bentley, E. Moskvin, S. Grigoriev, P. Fouquet, and B. Farago, Phys. Rev. Lett. **102**, 197202 (2009).

[6] S. Mühlbauer, B. Binz, F. Jonietz, C. Pfleiderer, A. Rosch, A. Neubauer, R. Georgii, and P. Böni, Science **323**, 915 (2009).

[7] H. Kawamura, Phys. Rev. Lett. **90**, 047202 (2003).

[8] Y. Taguchi, Y. Oohara, H. Yoshizawa, N. Nagaosa, and Y. Tokura, Science **291**, 2573 (2001).

[9] M. Onoda, G. Tatara, and N. Nagaosa, J. Phys. Soc. Jpn. **73**, 2624 (2004).

[10] P. Bruno, V. K. Dugaev, and M. Taillefumier, Phys. Rev. Lett. **93**, 096806 (2004).

[11] P. Bak and M. H. Jensen, J. Phys. C **13**, L881 (1980).

[12] O. Nakanishi, A. Yanase, A. Hasegawa, and M. Kataoka, Solid State Commun. **35**, 995 (1980).

[13] S. V. Maleyev, Phys. Rev. B **73**, 174402 (2006).

[14] K. Y. Ho, T. R. Kirkpatrick, Y. Sang, and D. Belitz, Phys. Rev. B **82**, 134427 (2010).

[15] U. K. Rössler, A. A. Leonov, and A. N. Bogdanov, J. Phys. Conf. Series **303**, 012105 (2011)

[16] H. Takizawa, T. Sato, T. Endo, and M. Shimada, J. Solid State Chem. **73**, 40 (1988).

[17] A. V. Tsvyashchenko, V. A. Sidorov, L. N. Fomicheva, V. N. Krasnorusski, and R. A. Sadikov (unpublished).

[18] N. Kanazawa, Y. Onose, T. Arima, D. Okuyama, K. Ohoyama, S. Wakimoto, K. Kakurai, S. Ishiwata, and Y. Tokura, Phys. Rev. Lett. **106**, 156603 (2011).

[19] A. V. Tsvyashchenko, J. Less-Common Met. **99**, L9 (1984).

[20] J. Rodriguez-Carvajal, Physica B **192**, 55 (1993); [http://www.ill.eu/sites/fullprof/].

[21] Assuming a regular helix, the value $\zeta = 4/25$ indicates an angle between Mn moments of $\theta = 57.6^\circ$ instead of 60° for $\zeta = 1/6$. In this context, the value $\theta = 60^\circ$ could be favored by a cubic anisotropy term in the (a,b) plane, since it allows more Mn moments to lock in the cubic axes. The more complex periodicity $\zeta = 4/25$ rather suggests a nonregular helix, and Fourier harmonics should yield high-order satellites, which have not been observed.

[22] B. Lebech, J. Bernhard, and T. Freltoft, J. Phys.: Condens. Matter **1**, 6105 (1989).

[23] Y. Ishikawa, K. Tajima, D. Bloch, and M. Roth, Solid State Commun. **19**, 525 (1976).

[24] T. Moriya, *Spin Fluctuations in Itinerant Magnetism* (Springer-Verlag, Berlin, 1985).

[25] R. D. Collyer and D. A. Browne, Physica B **403**, 1420 (2008).

[26] S. V. Grigoriev, S. V. Maleyev, V. A. Dyadkin, D. Menzel, J. Schoenes, and H. Eckerlebe, Phys. Rev. B **76**, 092407 (2007).

[27] S. V. Grigoriev, V. A. Dyadkin, E. V. Moskvin, D. Lamago, Th. Wolf, H. Eckerlebe, and S. V. Maleyev, Phys. Rev. B **79**, 144417 (2009).

[28] A. Herpin and P. Mériel, J. Phys. Radium **22**, 337 (1961); A. Yoshimori, J. Phys. Soc. Jpn. **14**, 807 (1959).

[29] N. Yamada, J. Phys. Soc. Jpn. **59**, 273 (1990).